


# Manipulation of Low-Frequency Sound with a Tunable Active Metamaterial Panel

Nan Gao<sup>1</sup>, Zhen Dong<sup>1</sup>, Ho Yiu Mak<sup>1</sup>, and Ping Sheng<sup>1\*</sup>

*Department of Physics, Hong Kong University of Science and Technology, Clear Water Bay, Kowloon, Hong Kong, China*

 (Received 25 January 2022; revised 11 March 2022; accepted 29 March 2022; published 20 April 2022)

We propose the design of a flat active wall panel and demonstrate its effectiveness in modulating the wall impedance, which can lead to the total absorption of incident sound waves in the low-frequency range of 50–120 Hz, or alter its reflection phase. Such an acoustic frequency range is usually the most difficult to handle for passive acoustic components, owing to the long wavelength, and consequently, the bulky size of the materials required. The active panel is actuated by a piezoelectric transducer, with its vibrational displacement amplified by a specially designed mechanical amplifier. Through both simulations and impedance-tube experiments, we show that simply tuning the active panel's displacement amplitude can vary its impedance from that of the hard wall, to impedance matching with air (leading to total absorption), to zero (leading to reflection phase reversal). No feedback loop is necessary for the active-panel device; only an initial adjustment during installation is necessary. We simulate the room-acoustics application for a  $1 \times 1$  m<sup>2</sup> wall panel that occupies only 1/48 of the total wall area of the room and show that it can introduce switchable elements to the audio experience.

DOI: [10.1103/PhysRevApplied.17.044037](https://doi.org/10.1103/PhysRevApplied.17.044037)

## I. INTRODUCTION

It is common knowledge that low-frequency noise, or, in general, low-frequency acoustic waves in the range of 50 to 100 Hz, is always the most difficult to either absorb or manipulate. The advent of artificial sound-absorbing materials, or metamaterials [1–13], has made it possible for effective sound attenuation, but such passive acoustic structures are still limited by the size of the structure, especially in the low-frequency range. Blocking or absorbing the low-frequency acoustic waves requires a thick sample size as dictated, respectively, by either the mass-density law or the causal minimum-sample thickness [14,15]. However, the slow rhythm of low-frequency acoustic waves offers an opportunity for active devices that can circumvent the limitations of the passive acoustic components. This is because low frequencies imply not only a lower power requirement for active devices, but also a diminished effect of the inevitable time delay due to the need for sensing the incident wave and processing the active response. As the acoustic characteristics of active devices can be tuned by electronic components, hence, they offer the potential of flexible tunability to suit application requirements [16–27].

For active sound extinction, active-noise-cancellation (ANC) technology represents a mature field [28–30]. It relies on the interference between incident noise waves

and actively emitted responding waves to cancel the noise within a given volume. In contrast to ANC, in this work, we propose an active-panel device that focuses on wall-impedance manipulations in the low-frequency range of 50 to 120 Hz that can not only totally absorb low-frequency sound, but also invert the reflection phase, as well as modulate the amplitude of the reflected wave. Owing to its flat-panel geometry, our active panels can be installed as part of a wall or ceiling to introduce switchable elements into room acoustics and its reverberation characteristics. In addition, different from the loudspeakers commonly used in ANC technology, here, we use a piezoelectric actuator, with a designed displacement amplifier, as the active component to attain the goal of surface-impedance tunability in room-acoustics applications [31,32], where the flat design is much desired. The operation of our active panel also requires no feedback loop. In the initial installation stage of the active panel, only the phase of the panel displacement needs to be adjusted to coincide with the incident wave and locked from that point of time onward. The amplitude of the displacement, on the other hand, can be continuously tuned to attain the desired effect, as detailed below.

In what follows, Sec. II first introduces the overall design strategy of the active-panel device, followed by the optimization strategy of the displacement amplifier. The process of experimental verification is then detailed. We use COMSOL simulations to delineate the application of the active panel in room acoustics in Sec. III, and conclude in

\*sheng@ust.hk

Sec. IV with a brief recapitulation of the salient features of this work.

## II. RESULTS

### A. Overall design strategy

#### 1. Intended effects

For a cuboid space shown in Fig. 1(a), consider an active panel with the same area placed opposite to the incident-wave side. The frequency, amplitude, and phase of the active panel are actuated in accordance with the known incident plane-wave signal, so that its impedance can satisfy either impedance matching to minimize the reflection or the soft boundary condition. That is,

$$Z_{\text{active}}/Z_0 = \begin{Bmatrix} 1 \\ 0 \end{Bmatrix}, \quad (1)$$

where  $Z_0$  is the impedance of air and  $Z_{\text{active}}$  is the impedance of the active wall. Here, one is for impedance matching, i.e., total absorption, and zero is for the soft boundary, which can lead to reflection phase inversion. The displacement velocity of the active panel is given by

$$v_{\text{active}} = kv_0 = k \frac{p_0}{\rho_0 c_0}, \quad (2)$$

where  $v_0$  is the displacement velocity of the incident wave,  $p_0$  denotes its pressure-modulation amplitude,  $\rho_0 = 1.225 \text{ kg/m}^3$  is the density of air, and  $c_0 = 340 \text{ m/s}$  is the speed of sound in air. Here,  $k$  is a parameter introduced to tune the displacement amplitude of the active panel, and we assume the active panel to have been tuned to move with the same phase as the incident wave. How that can be done is detailed below. When  $k = 1$ , the impedance-matching condition is satisfied, i.e.,  $Z_{\text{active}}/Z_0 = 1$ , so that there is no reflection; total absorption is achieved for the normally incident wave on the active panel. This is noted to differ from the ANC technology commonly used in active noise cancellation. In addition, another important function of the active wall is the realization of the soft-boundary condition, i.e.,  $Z_{\text{active}}/Z_0 = 0$ , which is a very important concept in the acoustic field [33]. This type of boundary impedance condition can be heuristically regarded as a virtual hard boundary that is extended quarter of a wavelength beyond the actual wall, thereby realizing phase inversion of the reflected wave in the same room position, as seen below. This characteristic makes it of great significance in practical applications in room acoustics, since the active panel can, for example, enhance the low-frequency sound pressure at a quarter-wavelength distance from the (actual) wall to alter the audio experience similar to that of a somewhat larger room. To realize the soft boundary, we just have to change the value of  $k$  to two. Under this displacement velocity amplitude, the impedance of the active panel is the soft boundary, created by the condition of

$\nabla \cdot \vec{v}_r = 0$  in the vicinity of active panel's surface, where  $\vec{v}_r$  denotes the displacement velocity in the comoving frame of the active panel, so that, in accordance with the mass-conservation law, the density and pressure modulations must both be zero. Details of the  $k = 2$  state are described in Text 1 within the Supplemental Material [34]. Under the soft-boundary condition, the reflected wave's phase becomes inverted from that of the incident wave. This is confirmed in subsequent simulations and experiment.

#### 2. Verification by simulations

Based on the above, we use the commercial finite-element software COMSOL to verify the intended effects for the simplified model, as shown in Fig. 1(a). Simulation details are given in Sec. V. In Fig. 1(b), we choose a plane-wave frequency of 50 Hz. By comparing the normalized sound-pressure amplitude on the surface of the active panel with different values of  $k$ , it can be found that, at  $k = 1$ , the active panel's surface-pressure amplitude is the same as that of the incident wave, and total absorption is achieved (since there is no reflection or transmission). At  $k = 2$ , the surface-pressure amplitude of the active panel is very close to zero, which means the soft-boundary condition. At  $k = 0$ , the active panel is stationary and acts as a hard wall.

The consequences of the altered boundary conditions can be verified by looking at the reflection coefficients, as shown in Fig. 1(c), in which the incident wave is chosen to comprise a combination of four different frequencies (50, 73, 92, and 120 Hz). The simulation results show that, when  $k$  changes from zero to one and then to two, the boundary can be regarded as varying from a stationary hard boundary to no reflection (total absorption) and then to phase inversion with the soft boundary, respectively.

#### 3. Time-domain operation

The active panel operates in the time domain by responding, with minimal delay, to the incident sound-wave train that can comprise a mixture of diverse frequencies. To restrict the actuation-frequency range of the active panel to the low-frequency operational range, the incident sound wave, converted into an electrical time series, is digitally filtered through a simple digital-convolution operation, to result in a filtered output time series that comprises only those frequencies in the active panel's operational range. Details of the digital-convolution filtering operation is detailed in Text 2 within the Supplemental Material [34].

#### 4. Sensing, time delay, and initial tuning of the active panel

An active device needs to have a sensor to "recognize" the incident sound and process this input to generate the

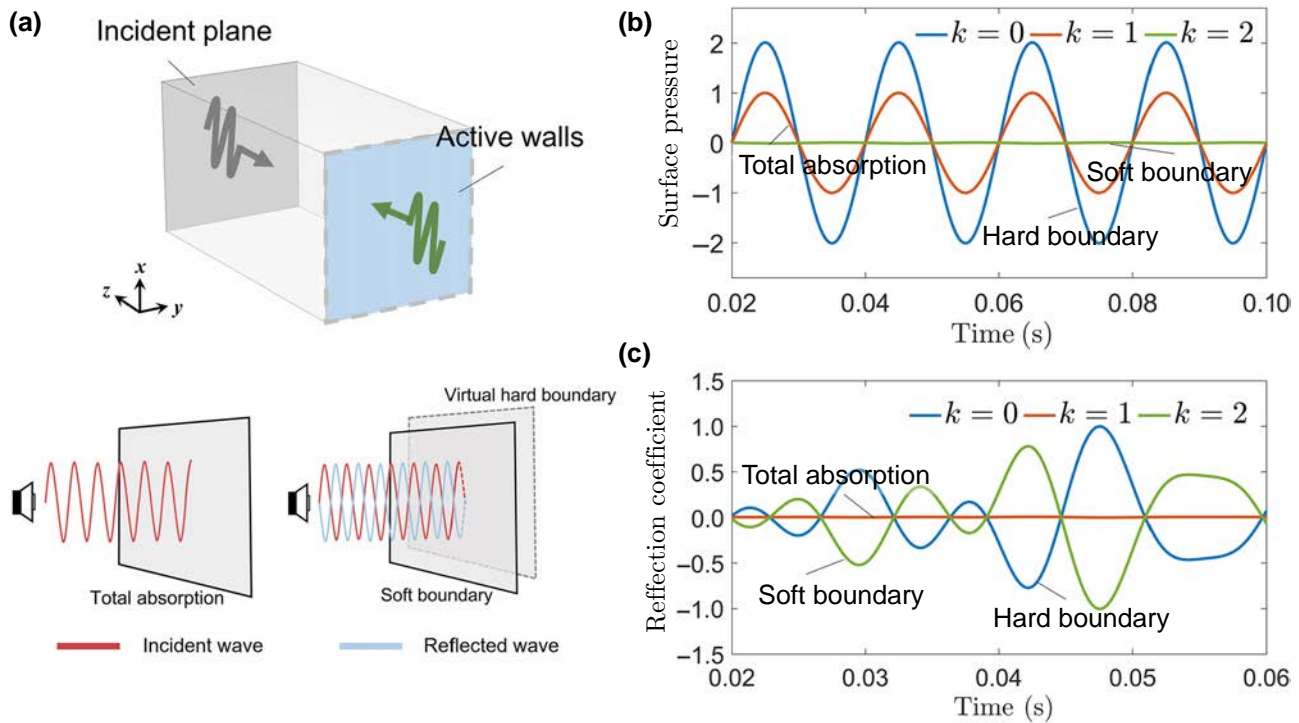


FIG. 1. Active panel and its intended effects. (a) Upper panel, schematic diagram of the active panel located opposite to the incident plane-wave source. Lower panel, on the left is an illustrated effect of total absorption with no reflection from the active wall panel. On the right is an illustrated effect of inverted phase of the reflected wave (drawn in blue line). Latter resembles the reflection from a virtual hard wall (shown by dashed border) situated a quarter of a wavelength beyond the actual wall. (b) Simulation results on the pressure amplitude at the surface of the active panel normalized by the incident sound. By varying the displacement amplitude factor,  $k$ , of the active panel at 50 Hz, it is shown that the boundary condition can be tuned. When  $k = 2$  (green line), the pressure amplitude is close to zero at the active-panel position, consistent with the soft-boundary condition. When the active panel is not moving, i.e.,  $k = 0$  (blue line), we have the hard-wall boundary condition, and the pressure amplitude is double that of the incident wave. (c) Simulation results showing the consequences of the altered boundary condition on the surface of the active panel. Here, we plot the reflection coefficient with multifrequencies, which shows that the effect of total absorption with no reflection at  $k = 1$ , and soft boundary with inverted phase at  $k = 2$ . For  $k = 0$ , the reflection coefficient is identical to that from the hard wall.

required actuation signal for the active device to respond. In the case of the active panel, the sensor is a small microphone, which can convert the sound source into an electrical time series. This time series will be filtered through a digital convolution, to restrict the actuation signal input to the active panel comprising only the low-frequency operational range. Since such digital processing requires some time duration, the response of the active panel may lag behind that of incident-wave arrival on the active panel, which is undesirable since, in that case, the active panel will not be able to be in the “in-phase” condition that is crucial for attaining the intended effects. To avoid such delay, it is imperative that the sensing microphone be placed close to the sound source, which is preferably at a distance between 1 and 3 m away from the active panel, so that the electrical signal can reach the actuation device ahead of the arrival of the incident sound wave, owing to the fact that the electrical signals travel much faster than the sound

wave. For a separation distance of 1 to 3 m between the sensor and the active panel, it would mean the electrical actuation signal could arrive 3 to 10 ms earlier, before the arrival of the incident sound wave at the active panel. The early arrival of the electrical signals implies that there can be time for digital processing and other inevitable time delays, as well as some leeway for phase adjustment of the active panel. In the case of diverse sound-source locations in a room, the sensing microphone should be placed in the middle of the room ceiling, and the active panel would only be able to respond to the synthesized sound train from diverse sources that reaches the microphone location.

When the active panel is initially installed, the in-phase condition of operation can be attained by using  $k = 1$ , i.e., minimum or no reflection condition, as the target by varying both the actuation signal’s amplitude and phase. Once the desired no-reflection condition—which can be determined by sensing the minimum in reflection—is

attained, the phase-actuation setting is locked for subsequent operations and only the amplitude setting, i.e., varying  $k$ , is allowed. In this manner, the active panel requires no feedback loops.

Our design is mainly targeted at low-frequency sound. For high-frequency acoustic waves, our active-panel design has some limitations, in terms of synchronization caused by the response-processing time delay and the increased input power. However, we note that, for high-frequency sound manipulation, passive acoustic metamaterials generally have excellent performance. Hence, for those cases requiring very broadband acoustic wave manipulations, we can use the advantage of the combination of active and passive control.

## B. Design of the active-panel device

We use piezoelectric ceramics as the actuator for the active panel; piezoelectric ceramic stacks (Coremorror NAC2021-H70-A01) are selected as the signal excitation

source. However, piezoelectric materials have the output characteristics of large force and small displacement. For the purpose of responding to low-frequency incident signals, large mechanical output displacement, usually much larger than what can be realized by the piezoelectric ceramic stacks, is required for the active panel. Hence, amplifying the output displacement of the piezoelectric ceramic stack is a key element in the active-panel design.

We design a mechanical displacement amplifier, shown in Fig. 2(a), to enhance the displacement of the input signal from the piezostack actuator. The mechanical amplifier is composed of a displacement output disk with a diameter of 8 cm (the disk is used to match the circular section waveguide in follow-up experiments) and three “legs” composed of 5-mm-thick stainless-steel thin plates, as shown in Fig. 2(b). During its operation, fixed constraints are applied at the positions labeled  $O_1$  and  $O_2$  of the amplifier, so that the whole structure can be regarded as a double-displacement amplification lever with fulcrums at  $O_1$  and  $O_2$ , leading to an order of magnitude

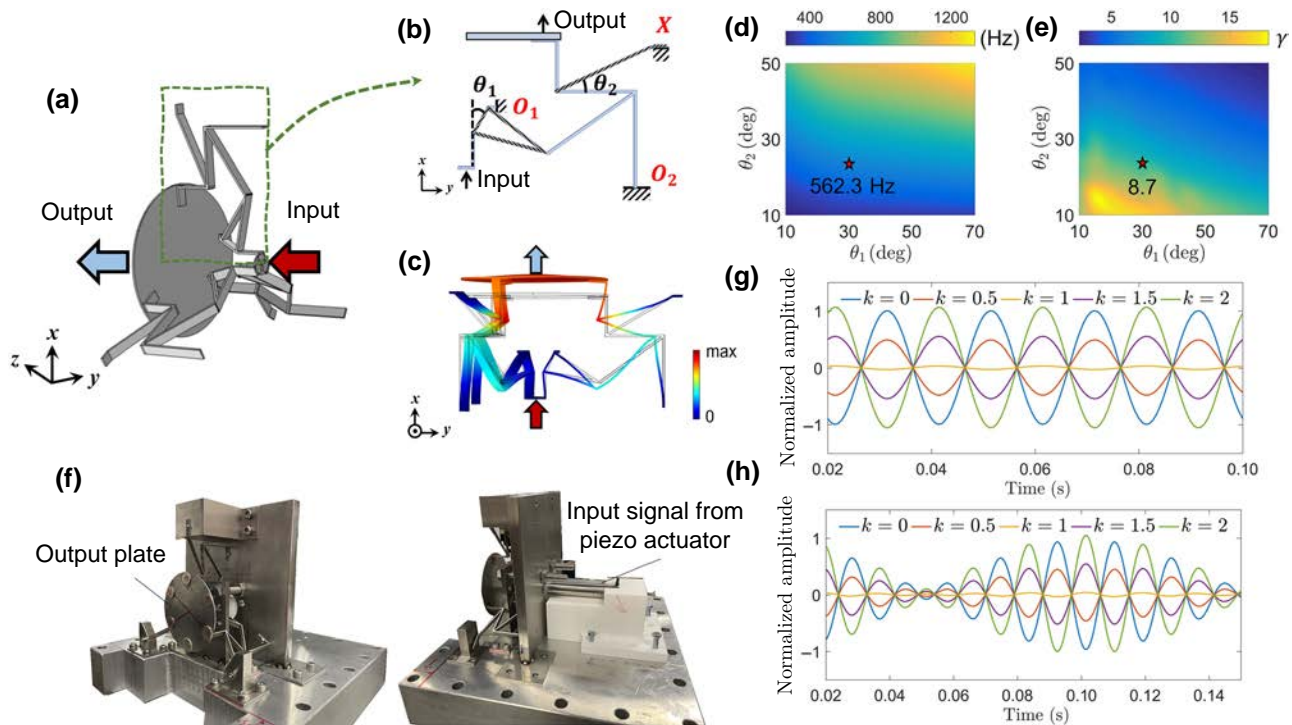


FIG. 2. Design of the displacement amplifier. (a) Schematic diagram of displacement amplifier. (b) Schematic diagram of one “leg,” as shown in the green box in (a), where positions  $O_1$ ,  $O_2$ , and  $X$  are applied with fixed constraints, and  $\theta_1$ ,  $\theta_2$  are the two geometric parameters that are to be optimized. (c) Input and output displacements of the amplifier, as indicated by color, where red represents the maximum displacement, and blue represents zero displacement, with in-between colors in the color bar indicating intermediate values of displacement. (d) Values of the first-order natural vibrational frequency of the amplifier plotted in color, as a function of  $\theta_1$  and  $\theta_2$ . Blue represents the minimum and yellow represents the maximum values. (e) Values of the amplification factor,  $\gamma$ , under 50-Hz incidence plotted in color as a function of  $\theta_1$  and  $\theta_2$ , where blue represents the minimum and yellow represents the maximum; schematic point indicated by the star is the final selected parameter combination; (f) photographs of the final design with a stainless-steel base; (g) single frequency and (h) multifrequency simulation results under different  $k$  with the displacement amplifier. In (g),(h), vertical axis denotes the simulated reflection amplitude normalized by the incident-wave amplitude, plotted as a function of time for various  $k$  values, as noted in each figure.

amplitude-amplification factor. However, since the displacement amplifier is a mechanical structure, we need to prevent its own natural vibration modes from affecting the stability and linearity of the displacement amplification. To this end, we need its first-order eigenfrequency to be higher than the working-frequency range. We add some additional thin legs [shaded parts in Fig. 2(b)] and apply a fixed constraint at the position labeled  $X$  to elevate the natural mechanical resonance frequency of the amplifier. The resulting displacement output of the amplifier is shown in Fig. 2(c), which shows that a small displacement velocity input at the bottom position can lead to a large (approximately a factor of 10) displacement velocity at the top output plate. We define an amplification factor,  $\gamma$ , as the ratio of the displacement velocity at the output plate,  $v_{\text{out}}$ , to the displacement velocity at the input position, i.e.,  $\gamma = v_{\text{out}}/v_{\text{in}}$ . Constancy in the value of  $\gamma$  as a function of frequency is essential to guarantee the linearity of the amplified output displacement at different frequencies.

During the operation of the amplifier, the input signal will inevitably lose part of its power to overcome the stiffness of the mechanical amplifier. To achieve a balance between the required high-amplification coefficient and the consequence of low natural frequency, which is undesirable, we select two geometric parameters,  $\theta_1$  and  $\theta_2$ , to optimize the design configuration. The simulation results on the first-order natural frequency of the amplifier, and the attendant amplification coefficient, are shown in Figs. 2(d) and 2(e), respectively, both plotted as a function of  $\theta_1$  and  $\theta_2$ . By considering a working frequency of 50–120 Hz in follow-up experiments,  $\theta_1 = 30^\circ$  and  $\theta_2 = 25^\circ$  are chosen. Under these material parameters, the stiffness of the overall structure is 5.96 MPa, the first natural frequency is 562.3 Hz, and the amplification factor is  $\gamma = 8.7$  at 50 Hz and  $\gamma = 9.1$  at 120 Hz. Hence, the amplification factor is very close to being a constant in the operating-frequency range, that is, the design has good linearity. This characteristic is better than that of a speaker horn with the same aperture size, because the latter will be affected by its own resonance frequency at low frequencies. Photographs of the final configuration are shown in Fig. 2(f). The whole amplifier is made of stainless steel with a Young's modulus of  $E = 195$  GPa, mass density of  $\rho = 7930$  kg/m<sup>3</sup>, and Poisson's ratio of  $\mu = 0.247$ . The displacement amplifier is fixed to the stainless-steel base with fasteners. In addition, the base is installed on the optical platform to maintain the stability of the whole device. Figures 2(g) and 2(h) show, respectively, the simulation results at the 50 Hz actuation input and dual-frequency superposition of 50 and 60 Hz input to the amplifier. As the simulations take into account the actual material parameters and geometric design of the mechanical amplifier, the results hereby verify the feasibility of the amplifier design (see Text 3 within the Supplemental Material for details of optimization and geometric parameters of the displacement amplifier [34]).

### C. Experimental realization of the active panel

To realize the intended effects of the active panel based on the above design, the vibration phase of the active panel must be consistent with the incident wave. Therefore, a sensor for picking up the incident signal needs to be set near the source, where the collected sound is converted into an electrical signal train and sent to the active panel's actuator, which can be some distance away from the sound source. Since the electrical signal travels much faster than the sound wave, the sensor's signals will arrive ahead of the sound wave. This difference in the arrival time offers room for the signal-processing time as well as phase adjustment for the actuator. Different from the ANC, which requires a complex feedback algorithm, our active wall needs only to adjust the phase and amplitude required for the impedance-matching condition.

Our experimental verification is carried out in a 1-m-long impedance tube with two sensing microphones set between the source and the active panel to process the sensed signals. The speaker source and the active panel are located at the two ends of the impedance tube; their phase difference is given by  $\Delta\varphi = 2\pi f(l_{\text{tube}}/c_0)$ , where  $f$  denotes the frequency and  $l_{\text{tube}} = 1$  m, so that  $\Delta\varphi \simeq 0.92$ – $2.2$  rad in the 50–120 Hz range. In addition, there is the inevitable time delay,  $\varphi_0$ , brought by the mechanical structure, which is about  $\varphi_0 = 1.17$ – $1.29$  rad in the same frequency range. In the experiment, we take the source to be the reference, i.e., as the zero phase, and the initial phase of the active panel should, therefore, be adjusted to be at the phase  $\varphi_{\text{active}} = \Delta\varphi + \varphi_0$ .

In actual operation, only the amplitude of the active plate i.e., changing the value of  $k$ , is needed to realize the tuning of different boundary situations. A schematic diagram illustrating the experiment setup is shown in Fig. 3(a). The speaker is at one end of the impedance tube and the circular active panel, about 9 cm in diameter, is at the other end. Two microphones, mic 1 and mic 2, are installed on the sidewall of the impedance tube. The distance between them and the end of the active panel is  $l_1 = 0.65$  m and  $l_2 = 0.1$  m, respectively. The two microphones are connected to the two channels of the oscilloscope, as well as to the two input channels of the lock-in amplifier after the conditioning amplifier. The former is to record the time-domain waveform signals, whereas the latter is to record the amplitude and phase information of the frequency-domain signal. A photograph of the experimental setups is shown in Fig. 3(b).

A functional signal generator is used to feed the sound speaker source, while, at the same time, it also feeds the same signal to the controller, which provides the necessary electrical inputs to the piezoelectric actuator, which, in turn, is the input to the mechanical amplifier used to actuate the active panel.

In the experiment, an adapter is fitted on the impedance tube first. A tensioned membrane is used to seal the gap

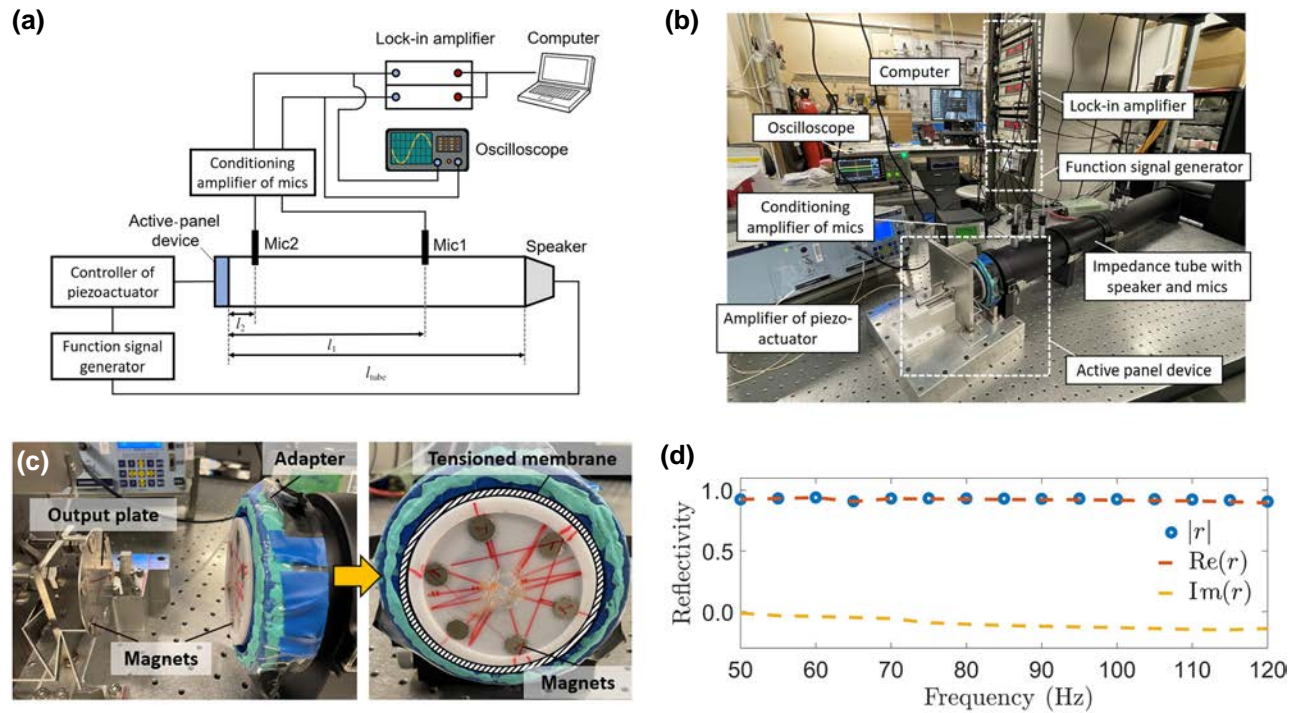


FIG. 3. Experimental setup of the active panel. (a) Schematic diagram of the experimental setup. (b) Photograph of the experiment setup, where the large white dotted square box delineates the active-panel device. (c) Photograph of the adapter that is fitted between the active panel and the end of the impedance tube. Active panel and output plate of the mechanical displacement amplifier are coupled by strong magnets. Gap between the active panel and impedance tube is sealed by a tensioned membrane, as shown by the shaded ring (right). (d) When  $k = 0$ , i.e., stationary hard boundary, experimental results on the reflectivity for frequencies between 50 and 120 Hz are shown by the red dashed line linking the blue open circles (real part). Yellow dashed line is the imaginary part of reflectivity. Reflection from the hard boundary serves as the reference case.

between the active panel and the impedance tube, as shown in the shaded ring (5 mm wide) of Fig. 3(c). The output plate of the mechanical displacement amplifier is coupled to the active panel by a ring of strong magnets. (See Text 4 within the Supplemental Material for the details of adapter fabrication with a tensioned membrane [34].) It should be noted that, for a tensioned membrane ring with a width of only 5 mm, the low-frequency sound pressure, in the frequency range of 50–120 Hz, cannot excite its eigenmodes. Therefore, the tensioned membrane is decoupled from the incident wave, i.e., it acts as a hard wall and completely reflects the incident wave.

To verify the hard-boundary reflection at  $k = 0$ , we sweep the frequency in the range of 50–120 Hz, and the results are shown in Fig. 3(d). It is seen that the real part of the reflectivity,  $\text{Re}(r)$ , is close to one, whereas the imaginary part,  $\text{Im}(r)$ , is close to zero. The magnitude of  $r$  is very close to one, as expected.

By using the above-described setup, we verify the two cases of  $k = 1$  and  $k = 2$ . The dual microphones are used to measure the reflected wave in the time domain. In the experiment, the source and the active panel are fed a single-frequency sine wave, with the phase of the active wall set at  $\varphi_{\text{active}}$ , as noted above. The displacement

amplitude of the active panel is tuned so that the effect of total absorption is attained. The relevant amplitude setting is labeled as  $k = 1$  for this state. By locking the initial phase of the active panel and doubling the amplitude setting, we attain the case of  $k = 2$  for the soft-boundary impedance effect.

Two channels associated with the same signal generator are used to send signals at the same time, to ensure the synchronization of the input signals. From the signals of the two sensing microphones of the impedance tube, the frequency-domain information, i.e., the amplitude and phase at the two microphone positions, is obtained by the lock-in amplifier to evaluate the reflection coefficient and other correlation coefficients. The oscilloscope is used to display steady-state waveforms. Details of time-domain- and frequency-domain-signal measurement approaches can be found in Texts 5 and 6 within the Supplemental Material [34].

In Figs. 4(a)–4(c), we show the waveforms of the source and measured reflected waves when  $k = 1$  at a frequency of 50, 70, and 120 Hz, respectively. It is seen that the reflected wave is almost zero. In Figs. 4(d)–4(f), we show the waveforms of the source and measured reflected waves when  $k = 2$  at the same three frequencies. It is seen that

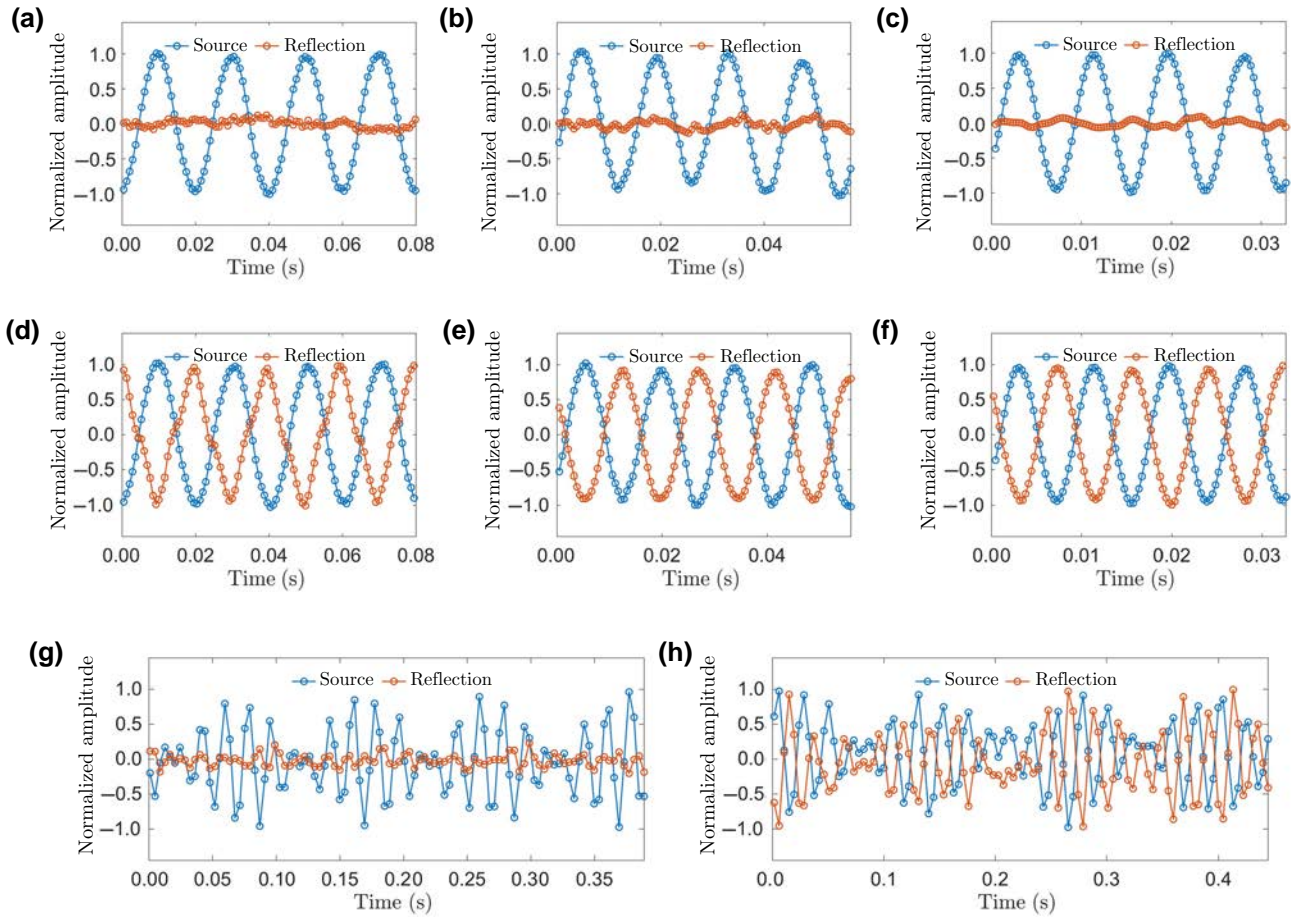


FIG. 4. Experimental results in the time domain, plotted in terms of the measured amplitude normalized by the amplitude of the incident wave. (a)–(c) Source and reflected waveforms when  $k = 1$ , at 50, 70, and 120 Hz, respectively. It is seen that the reflected-wave amplitude is close to zero, as expected. (d)–(f) Source and reflected waveforms when  $k = 2$ , at 50, 70, and 120 Hz, respectively. It is seen that the reflected waveform is  $180^\circ$  inverted from the incident wave. (g),(h)  $k = 1$  and  $k = 2$  cases, respectively, for the dual-frequency combination (50 and 60 Hz). Here, blue open circles represent the waveform of the source, and red open circles represent the reflected waveform. It is seen that the reflected waveform is close to zero in (g), whereas the reflected waveform is phase inverted in (h). All results are normalized to the maximum value of the source amplitude. Zero point on the time axis represents the reference point for displaying data.

the amplitudes of the reflected wave are close to that of the source, but the phase is reversed, i.e., the soft-boundary impedance is attained by the active panel. In Figs. 4(g) and 4(h), we display the same  $k = 1$  and  $k = 2$  active-panel effect with the superposition of 50 and 60 Hz. Both the total absorption and soft-boundary effects are fairly accurately reproduced in the time domain. Thus, the experimental results prove the feasibility of using the active panel to realize total absorption and a soft boundary with impedance modulation. In the following, we use simulations to demonstrate the room-acoustic applications of the active panel.

It should be noted that the working input power to the piezoelectric actuator is less than 5 W. The required power is positively correlated with the operating frequency, i.e., higher frequencies require higher power. However, at our low-frequency regime, 5 W is not the total required power,

as the electronic components of the piezoelectric stack consume power as well; hence, the total power may be somewhat higher.

### III. SIMULATIONS ON ROOM-ACOUSTIC APPLICATIONS

We simulate the effects of a  $1 \times 1 \text{ m}^2$  active panel placed on the wall of a room with dimensions of 3 m (width)  $\times$  3 m (depth)  $\times$  2.5 m (height), as shown in Fig. 5(a) (active panel is indicated by blue shading). Our simulations are carried out with a single monopole sound point source,  $S$ , placed at the center position of the wall opposite to the active panel, at a distance of 10 cm from the wall. The point source emits spherical waves with frequencies of 50 and 120 Hz, with a sound-power level of 95 dB. The distance between the sound source and the active

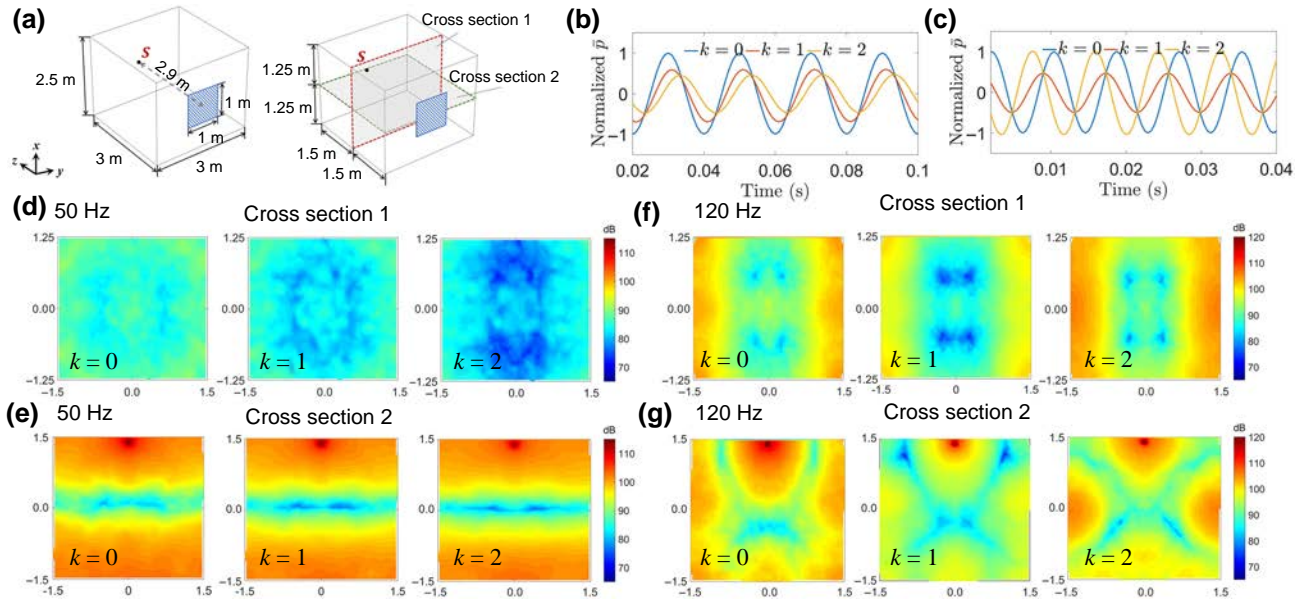


FIG. 5. Simulation results for room-acoustic application of a  $1 \times 1 \text{ m}^2$  active panel. (a) (Left panel) Schematics of  $3 \times 3 \times 2.5 \text{ m}^3$  enclosed room with a point sound source placed 10 cm away from the center of the wall.  $1 \times 1 \text{ m}^2$  active panel is placed in the middle of the opposite wall (indicated by blue shading). Point source  $S$  is located 2.9 m away from the active panel. (Right panel) Cross sections 1 and 2 are set to pass through the center of the room and are set parallel to the  $x$ - $y$  plane and  $y$ - $z$  plane, respectively, as the observation cross-section surfaces of the subsequent sound-field distribution. Given the incident wave and vibration excitation of point source and active plate with frequencies of (b) 50 Hz and (c) 120 Hz, time-domain variations of room-averaged sound pressure under different amplitude factors,  $k$ , in which the blue line denotes  $k = 0$ , red line denotes  $k = 1$ , and the yellow one represents  $k = 2$ . Sound-pressure amplitude is standardized according to the maximum value at  $k = 0$ . Amplitude of sound pressure is extracted to calculate the sound-pressure levels at two cross sections, in SPL, where (d),(e) are the SPL distributions of cross sections 1 and 2 at 50 Hz with  $k = 0 - 2$ , respectively, and (f),(g) are the result of two cross sections at 120 Hz. Here, in cross section 2, the source is noted by a black dot at top center.

panel is 2.9 m. Other than the active panel, all the walls are assumed to have hard-boundary conditions. To better display the distribution of the indoor sound field under different conditions, we set two sections passing through the center of the room, namely, cross section 1 parallel to the  $x$ - $y$  plane and cross section 2 parallel to the  $y$ - $z$  plane [see the shaded parts on the right panel of Fig. 5(a)].

Due to the use of the point source, the emitted sound can arrive at the active panel after multiple scatterings from the wall. Hence, all the simulations are conducted in the time domain to accurately account for the interaction of the active panel with the sound field at every instant of time.

In actual room-acoustic applications, a microphone sensor should be placed near the source to pick up the sound emitted by the source and transmit it electrically to the active-panel controller after digital processing by the electronic filter (see the Supplemental Material for a description of signal filtering [34]). The resulting output-electrical-signal time series would have the frequency content in the relevant low-frequency range of the active-panel operation. Since the electrical signals arrive at the opposite wall earlier than the emitted sound wave, this time difference can be used for digital processing, as well as for phase adjustment.

To simplify the simulations in this work, we assume that the above phase adjustment is already done, so that we can focus on the effects of the active panel that has an area  $1/48$  of the total wall area (including the ceiling and floor).

For room acoustics, the wave phenomena are closely related to the relative ratio between the wavelength of the source wave and the size of the room. We define a characteristic length of the room as  $l_0 = \sqrt[3]{V}$ , and its corresponding characteristic frequency,  $f_0$ , as

$$f_0 = \frac{c_0}{l_0}. \quad (3)$$

In the present model,  $f_0 \cong 121.5 \text{ Hz}$  serves as a standardized quantity for the subsequent analysis. When the walls of the rectangular room are all hard-boundary conditions, the lowest nonzero eigenfrequency is  $0.47f_0$  or about 57 Hz. When the walls are all soft sound boundaries, the lowest eigenfrequency is  $0.87f_0$  or about 106 Hz [35] (see Text 2 within the Supplemental Material for a description of signal filtering [34]). Hence, for a 50-Hz incident wave, its frequency is lower than the lowest eigenfrequency of the room, and the eigenmode of the room would not be able to be excited. For the 120-Hz incident wave, its frequency



is higher than the lowest eigenfrequency. Hence, in the case of these two frequencies, the introduction of the active wall will bring different effects for the room's sound field.

When the source emits an incident wave of 50 Hz, we set the phase of the active panel in accordance with the direct distance to the source and set its amplitude to be consistent with the source as well, so that, when the incident wave reaches the active panel, it will meet the impedance-matching condition for direct arrival. We regard this condition to be  $k = 1$ . After tuning the value of  $k$  from zero to two, the average amplitude of the room's sound pressure, in the time domain, is shown in Fig. 5(b). The results show that, when  $k = 1$ , the average sound-pressure amplitude is close to half of that when  $k = 0$ . This means an averaged reduction of 7.6 dB in sound-pressure level (SPL) in the low-frequency range with only 1/48 of the total wall area.

When  $k = 2$ , the volume-averaged pressure amplitude is slightly less than that for  $k = 1$ . In addition, the overall phase has a nearly  $90^\circ$  shift compared to the  $k = 0$  case. The phase shift cannot be  $180^\circ$  because not all the arrivals are like that in the impedance tube, i.e., direct arrival. Nevertheless, a  $90^\circ$  average phase shift can greatly alter the indoor auditory experience. The average SPL distributions of the two cross sections in the center of the room are shown in Figs. 5(d) and 5(e). It can be clearly observed that the sound-pressure level changes significantly at the central position of the room with the change in the vibration amplitude of the active panel, and the SPL can be reduced by nearly 10 dB at some positions.

For an incident wave of 120 Hz, it will be able to excite the resonance modes of the room, thereby making the situation of the indoor sound field a bit closer to that of reverberation. In this case, the phase and amplitude of the two important parameters of the active panel are set by adjusting parameters to target the condition of  $k = 1$ , i.e., "maximum absorption," which means changing the parameters of the active panel to reach the *lowest average sound pressure* and regarding this condition as  $k = 1$ . Doubling the amplitude of the panel is then regarded as the condition for  $k = 2$ . Based on such parameter settings, the simulated average sound-pressure amplitude in the room is displayed in Fig. 5(c), which can obviously show that the effect of the active wall is different from that of the 50-Hz case. When  $k = 1$ , the indoor average sound pressure is the smallest, yielding an averaged reduction of 8.6-dB SPL. Interestingly, the pressure-amplitude values of  $k = 2$  and  $k = 0$  are very close, but their phases have an offset of about  $130^\circ$ , which is closer to the "soft-boundary" effect than that for the 50-Hz case. Such results can also be reflected in the sound-pressure-level distribution of two central cross sections, as shown in Figs. 5(f) and 5(g). From the perspective of wave propagation, whether the incident wave is direct arrival or having the characteristic of reverberation after multiple scattering, there is always a certain probability for

the emitted wave to fall within the physical range of the active plate. The minimum sound-pressure value obtained after parameter tuning is the result of reducing the reflected waves by the best impedance matching of the sound wave falling within the area of the active panel.

There is a heuristic reason why the  $k = 1, 2$  states of the active panel can be so effective, even with such a small area fraction of the total wall area. We observe that the active panel's impedance is in *parallel* with the rest of the hard-wall impedance. Hence, in accordance with the rule of parallel addition of the impedance, the effective impedance of the whole wall, including that of the active panel, should be

$$\frac{1}{\tilde{Z}} = \frac{\eta}{Z_{\text{act}}} + \frac{1 - \eta}{Z_{\text{hard}}}, \quad (4)$$

where  $\tilde{Z}$  denotes the effective impedance of the whole wall,  $\eta$  is the area fraction of the active panel with impedance  $Z_{\text{act}}$ , and  $Z_{\text{hard}}$  is the hard-wall impedance for the remainder of the wall. Since  $Z_{\text{hard}} \gg Z_{\text{act}}$  for either  $k = 1$  or  $2$ , it is clear that even if  $\eta$  is small, the active panel can still have a large effect on  $\tilde{Z}$ .

To sum up, the active panel, which occupies only 1/48 of the indoor surface area, can have a very significant effect on the regulation of the room's sound field in the low-frequency range. It can realize not only the function of noise reduction, but also the average phase of the sound field, so that there can be a different auditory experience for low-frequency sound, which may have an important reference value for the design of indoor environments with specific acoustic needs.

#### IV. CONCLUSIONS

Here, we propose an active-panel device that can realize the flexible and effective manipulation of wall impedance in the low-frequency range of 50–120 Hz by adjusting its displacement amplitude, to realize the effect of either total sound absorption or a soft boundary. The effects are verified by both simulations and experiments. In the design of the active-panel device, a piezoelectric actuator and a designed mechanical displacement amplifier are combined to affect the tunable pistonlike vibrational output and realize the goal of impedance modulation. Among them, the structure of the displacement amplifier is composed of multiple slender thin metal sheets. By imposing fixed constraints on the specified positions, we realize the function of displacement amplification with a certain stiffness. After optimization, the design is shown to be unaffected by its own natural frequency within the working-frequency range. In addition, the potential application of the active panel in room acoustics is analyzed by simulations. The results show that a small-sized active panel can achieve a very significant sound-field-manipulation effect in a relatively large space. In particular, it can not only reduce

low-frequency noise, but also realize an average phase shift of the sound field, which can significantly alter room occupants' auditory experiences. Our results provide a reference for the design and application of a room's acoustic metamaterials.

## V. METHODS

### A. Measurement setup

The displacement amplifier is made of stainless steel by computer numerical controlled machining and welding. The experimental setting is shown in Fig. 3(b). The two channels of the signal generator (Keysight 33500B) are, respectively, connected with the loudspeaker of the impedance tube (B&K 4206) and the piezocontroller (Coremorrow E00.C2). They are then connected to the piezoactuator (Coremorrow NAC2021-H70-A01). The two microphones of the impedance tube are divided into two channels through the conditioning amplifier of microphones (B&K Type 2693-A), one being connected to the lock-in amplifier (SR830) and the other being connected to the oscilloscope (Keysight EDUX1002G). The former is used to obtain frequency-domain data, and the latter is used to obtain the time-domain signal.

### B. Numerical simulations

All simulation works are carried out by using COMSOL 5.5 Multiphysics. Among them, the time domain and frequency domain of solid mechanic modules are used for the design of the displacement amplifier (Sec. II B), the pressure-acoustic and solid-mechanic-coupling module is also used in this part, and the time domain of the pressure-acoustic module is used for the simulation of room acoustics (Sec. III).

## ACKNOWLEDGMENTS

P.S. wishes to acknowledge the research funding support of A-HKUST601/18 for this work. N.G. sincerely thanks Walter Ho and William Wong for fabrication of the displacement amplifier and its base.

The authors declare no conflict of interest.

- 
- [1] J. Mei, G. Ma, M. Yang, Z. Yang, W. Wen, and P. Sheng, Dark acoustic metamaterials as super absorbers for low-frequency sound, *Nat. Commun.* **3**, 756 (2012).
  - [2] N. Gao, S. Qu, J. Li, J. Wang, and W. Chen, Harnessing post-buckling deformation to tune sound absorption in soft helmholtz absorbers, *Int. J. Mech. Sci.* **208**, 106695 (2021).
  - [3] N. Jiménez, W. Huang, V. Romero-García, V. Pagneux, and J.-P. Groby, Ultra-thin metamaterial for perfect and quasi-omnidirectional sound absorption, *Appl. Phys. Lett.* **109**, 121902 (2016).

- [4] H. Long, Y. Cheng, and X. Liu, Asymmetric absorber with multiband and broadband for low-frequency sound, *Appl. Phys. Lett.* **111**, 143502 (2017).
- [5] J. Boulvert, J. Costa-Baptista, T. Cavalieri, V. Romero-García, G. Gabard, E. R. Fotsing, A. Ross, M. Perna, J. Mardjono, and J.-P. Groby, Folded metaporous material for sub-wavelength and broadband perfect sound absorption, *Appl. Phys. Lett.* **117**, 251902 (2020).
- [6] S. M. Montgomery, S. Wu, X. Kuang, C. D. Armstrong, C. Zemelka, Q. Ze, R. Zhang, R. Zhao, and H. J. Qi, Magneto-mechanical metamaterials with widely tunable mechanical properties and acoustic bandgaps, *Adv. Funct. Mater.* **31**, 2005319 (2021).
- [7] Z. Cai, S. Zhao, Z. Huang, Z. Li, M. Su, Z. Zhang, Z. Zhao, X. Hu, Y. Wang, and Y. Song, Bubble architectures for locally resonant acoustic metamaterials, *Adv. Funct. Mater.* **29**, 1906984 (2019).
- [8] V. Romero-García, N. Jimenez, G. Theocharis, V. Achilleos, A. Merkel, O. Richoux, V. Tournat, J.-P. Groby, and V. Pagneux, Design of acoustic metamaterials made of helmholtz resonators for perfect absorption by using the complex frequency plane, *C. R. Phys.* **21**, 713 (2020).
- [9] K. Zhang, C. Ma, Q. He, S. Lin, Y. Chen, Y. Zhang, N. X. Fang, and X. Zhao, Metagel with broadband tunable acoustic properties over air–water–solid ranges, *Adv. Funct. Mater.* **29**, 1903699 (2019).
- [10] J. Li, X. Wen, and P. Sheng, Acoustic metamaterials, *J. Appl. Phys.* **129**, 171103 (2021).
- [11] S.-H. Park, Acoustic properties of micro-perforated panel absorbers backed by Helmholtz resonators for the improvement of low-frequency sound absorption, *J. Sound Vib.* **332**, 4895 (2013).
- [12] A. Elayouch, M. Addouche, and A. Khelif, Extensive tailorability of sound absorption using acoustic metamaterials, *J. Appl. Phys.* **124**, 155103 (2018).
- [13] M. Amin, O. Siddiqui, M. Farhat, and A. Khelif, A perfect fresnel acoustic reflector implemented by a fano-resonant metascreen, *J. Appl. Phys.* **123**, 144502 (2018).
- [14] M. Yang, S. Chen, C. Fu, and P. Sheng, Optimal sound-absorbing structures, *Mater. Horiz.* **4**, 673 (2017).
- [15] M. Yang and P. Sheng, An integration strategy for acoustic metamaterials to achieve absorption by design, *Appl. Sci.* **8**, 1247 (2018).
- [16] B.-I. Popa, D. Shinde, A. Konneker, and S. A. Cummer, Active acoustic metamaterials reconfigurable in real time, *Phys. Rev. B* **91**, 220303 (2015).
- [17] B.-I. Popa, L. Zigoneanu, and S. A. Cummer, Tunable active acoustic metamaterials, *Phys. Rev. B* **88**, 024303 (2013).
- [18] Y. Wang, Y. Wang, B. Wu, W. Chen, and Y. Wang, Tunable and active phononic crystals and metamaterials, *Appl. Mech. Rev.* **72**, 040801 (2020).
- [19] Y. Liao, X. Zhou, Y. Chen, and G. Huang, Adaptive metamaterials for broadband sound absorption at low frequencies, *Smart Mater. Struct.* **28**, 025005 (2018).
- [20] S. Zhao, A. Chen, Y. Wang, and C. Zhang, Continuously Tunable Acoustic Metasurface for Transmitted Wavefront Modulation, *Phys. Rev. Appl.* **10**, 054066 (2018).
- [21] C. Cho, X. Wen, N. Park, and J. Li, Acoustic willis meta-atom beyond the bounds of passivity and reciprocity, *Commun. Phys.* **4**, 82 (2021).

- [22] M. Furstoss, D. Thenail, and M.-A. Galland, Surface impedance control for sound absorption: Direct and hybrid passive/active strategies, *J. Sound Vib.* **203**, 219 (1997).
- [23] T. T. Koutserimpas, E. Rivet, H. Lissek, and R. Fleury, Active Acoustic Resonators with Reconfigurable Resonance Frequency, Absorption, and Bandwidth, *Phys. Rev. Appl.* **12**, 054064 (2019).
- [24] G. Ma, X. Fan, P. Sheng, and M. Fink, Shaping reverberating sound fields with an actively tunable metasurface, *Proc. Natl. Acad. Sci. U. S. A.* **115**, 6638 (2018).
- [25] W. Akl and A. Baz, Experimental characterization of active acoustic metamaterial cell with controllable dynamic density, *J. Appl. Phys.* **112**, 084912 (2012).
- [26] A. Sasmal, N. Geib, B.-I. Popa, and K. Grosh, Broadband nonreciprocal linear acoustics through a non-local active metamaterial, *New J. Phys.* **22**, 063010 (2020).
- [27] Y. Zhai, H.-S. Kwon, and B.-I. Popa, Active willis metamaterials for ultracompact nonreciprocal linear acoustic devices, *Phys. Rev. B* **99**, 220301 (2019).
- [28] H. Huang, X. Qiu, and J. Kang, Active noise attenuation in ventilation windows, *J. Acoust. Soc. Am.* **130**, 176 (2011).
- [29] S. M. Kuo and D. R. Morgan, *Active Noise Control Systems* (Wiley, New York, 1996). Vol. 4.
- [30] S. J. Elliott and P. A. Nelson, Active noise control, *IEEE Signal Process. Mag.* **10**, 12 (1993).
- [31] S. Qu and P. Sheng, Minimizing Indoor Sound Energy with Tunable Metamaterial Surfaces, *Phys. Rev. Appl.* **14**, 034060 (2020).
- [32] P. Zhang, C. Cong, J. Tao, and X. Qiu, Dual frequency sound absorption with an array of shunt loudspeakers, *Sci. Rep.* **10**, 10806 (2020).
- [33] H. Y. Mak, X. Zhang, Z. Dong, S. Miura, T. Iwata, and P. Sheng, Going Beyond the Causal Limit in Acoustic Absorption, *Phys. Rev. Appl.* **16**, 044062 (2021).
- [34] See the Supplemental Material at <http://link.aps.org/supplemental/10.1103/PhysRevApplied.17.044037> for details of simulations and experiments for this work.
- [35] H. Kuttruff, *Room Acoustics* (CRC Press, Boca Raton, 2016).